Experimental Eye Research 207 (2021) 108600

Contents lists available at ScienceDirect

Experimental Eye Research

journal homepage: www.elsevier.com/locate/yexer

Intravitreal gene therapy protects against retinal dysfunction and degeneration in sheep with CLN5 Batten disease

Samantha J. Murray [a], Katharina N. Russell [a], Tracy R. Melzer [e], Steven J. Gray [b], Stephen J. Heap [c], David N. Palmer [a,d], Nadia L. Mitchell [a,d,*]

[a] Faculty of Agricultural and Life Sciences, Lincoln University, Lincoln, 7647, New Zealand
[b] Department of Pediatrics, University of Texas Southwestern Medical Center, Dallas, TX, 75390, USA
[c] McMaster & Heap Veterinary Practice, Christchurch, 8025, New Zealand
[d] Department of Radiology, University of Otago, Christchurch, 8140, New Zealand
[e] Department of Medicine, University of Otago, Christchurch and the New Zealand Brain Research Institute, Christchurch, 8011, New Zealand

ARTICLE INFO

Keywords:
Neuronal ceroid lipofuscinosis
Sheep
Intravitreal
Electroretinography
Gene therapy
AAV9
CLN5
CLN6

ABSTRACT

Neuronal ceroid lipofuscinoses (NCL; Batten disease) are a group of inherited neurodegenerative diseases primarily affecting children. A common feature across most NCLs is the progressive loss of vision. We performed intravitreal injections of self-complementary AAV9 vectors packaged with either ovine *CLN5* or *CLN6* into one eye of 3-month-old *CLN5*$^{-/-}$ or *CLN6*$^{-/-}$ animals, respectively. Electroretinography (ERG) was performed every month following treatment, and retinal histology was assessed post-mortem in the treated compared to untreated eye. In *CLN5*$^{-/-}$ animals, ERG amplitudes were normalised in the treated eye whilst the untreated eye declined in a similar manner to CLN5 affected controls. In *CLN6*$^{-/-}$ animals, ERG amplitudes in both eyes declined over time although the treated eye showed a slower decline. Post-mortem examination revealed significant attenuation of retinal atrophy and lysosomal storage body accumulation in the treated eye compared with the untreated eye in *CLN5*$^{-/-}$ animals. This proof-of-concept study provides the first observation of efficacious intravitreal gene therapy in a large animal model of NCL. In particular, the single administration of AAV9-mediated intravitreal gene therapy can successfully ameliorate retinal deficits in *CLN5*$^{-/-}$ sheep. Combining ocular gene therapy with brain-directed therapy presents a promising treatment strategy to be used in future sheep trials aiming to halt neurological and retinal disease in CLN5 Batten disease.

1. Introduction

Neuronal ceroid lipofuscinoses (NCL; Batten disease) are a group of fatal inherited neurodegenerative diseases of childhood with a prevalence of up to 1 in 12,500 live births (Rider et al., 1988). Currently 13 variants of NCL have been identified (CLN1-8, 10–14), all resulting from different genetic mutations but typically with a shared disease phenotype (Mole and Cotman, 2015). A pathological hallmark of NCL is the accumulation of lysosome-derived storage bodies in cells throughout the body, including neuronal cells of the brain (Cooper et al., 2015). There is also widespread brain atrophy, retinal degeneration and heightened neuroinflammation. Affected children progressively develop blindness, motor degeneration, epilepsy and dementia, eventually reaching total dependency and premature death (Kousi et al., 2012; Mole et al, 2005, 2011). Medications are commonly used to manage symptoms but few effective disease-modifying therapies exist for NCL (Kohlschütter et al., 2019; Williams et al., 2017). There is only one clinically approved enzyme-replacement therapy for the CLN2 disease and several brain-directed gene- and enzyme-replacement therapies are currently showing promise in clinical trials (Mole et al., 2019) however none of these directly address the retinal degeneration and vision loss observed across all forms of NCL.

Batten disease occurs naturally in many other mammals, including a CLN5 form in Borderdale sheep (Frugier et al., 2008; Jolly et al., 2002), and a CLN6 form in South Hampshire sheep (Jolly and West, 1976; Tammen et al., 2006). Sheep with CLN5 or CLN6 Batten disease display a similar disease course to the human condition, with progressive blindness, stereotypical motor deficits, reduced mentation and premature death before two years of age (Jolly et al, 1989, 2002, 1989; Mayhew et al., 1985; Mitchell et al., 2018). Affected sheep also have severe

* Corresponding author. Faculty of Agricultural and Life Sciences, PO Box, 85084, Lincoln University Lincoln, 7647, Canterbury, New Zealand.
E-mail address: Nadia.Mitchell@lincoln.ac.nz (N.L. Mitchell).

https://doi.org/10.1016/j.exer.2021.108600
Received 22 September 2020; Received in revised form 12 April 2021; Accepted 21 April 2021
Available online 28 April 2021

cortical atrophy, neuroinflammation, and accumulation of lysosomal storage, mirroring the human disease post-mortem (Mitchell et al., 2018; Oswald et al., 2005).

Blindness in NCL consists of a central and a peripheral component, as both the occipital lobe and the retina are affected. A significant reduction in the grey matter thickness of the primary visual cortex has been reported for both forms of ovine NCL (Jolly et al., 2002; Mitchell et al., 2018; Oswald et al., 2005). In both humans and sheep, retinal atrophy results from an almost complete loss of rod and cone photoreceptors, as well as cells in the outer nuclear layer (ONL), whereas the inner layers of the retina are relatively spared (Goebel et al., 1974; Graydon and Jolly, 1984; Jolly et al., 1982; Mayhew et al., 1985). Lysosomal storage is observed in the ganglion cell layer (GCL) and retinal pigment epithelium (RPE), and there is evidence of gliosis throughout the retina and the optic nerve (Goebel et al, 1974, 1982, 1974; Radke et al., 2015). Abnormal or abolished electroretinography (ERG) recordings have been reported for most forms of human NCL (Harden and Pampiglione, 1982; Weleber, 1998; Weleber et al., 2004), and also more recently for the ovine CLN5 and CLN6 diseases (Russell et al., 2021). Given CLN5 and CLN6 affected sheep eyes exhibit similar loss of function and histopathology to human patients, these sheep represent an ideal model in which to perform a proof-of-concept study of intravitreal gene therapy.

Intracerebroventricular delivery of *CLN5* packaged in an adeno-associated virus (AAV) has been shown to halt stereotypical disease progression in the CLN5 sheep model, however the animals still lost their sight, albeit later than if no treatment is given (Mitchell et al., 2018). This suggests that while brain-directed gene therapy can attenuate cortical atrophy and associated clinical signs, the therapy does not reach the eye in sufficient quantities to protect the retina. Similar observations have been noted following brain-directed gene therapy in other animal models of NCL (Katz et al., 2015; Sondhi et al., 2013; Whiting et al., 2016).

It is estimated that more than 80% of the information that the brain receives comes from the visual system. Visual dysfunction can negatively impact on human lifestyle and significantly lower the quality of life. AAV-mediated intravitreal gene therapy approaches have been tested in models of inherited retinal neurodegeneration with positive outcomes leading to several clinical trials, including gene therapies for Leber's hereditary optic neuropathy (ClinicalTrials.gov NCT02652780) and X-linked retinoschisis (ClinicalTrials.gov NCT02416622). Here, in a proof-of-concept study, we show that the intravitreal (IVT) administration of AAV9-mediated gene therapy in pre-symptomatic NCL sheep affords protection against retinal dysfunction, degeneration, inflammation, and the accumulation of pathological lysosomal storage.

2. Methods

2.1. Animals

Borderdale and South Hampshire sheep were diagnosed at birth (Frugier et al., 2008; Tammen et al., 2006) and maintained at the Lincoln University research farm under US National Institutes of Health guidelines for the care and use of animals in research and the NZ Animal Welfare Act (1999). All experimental protocols were approved by the Lincoln University Animal Ethics Committee. Six pre-symptomatic 3-month-old ewes, consisting of three *CLN5*$^{-/-}$ Borderdales and three *CLN6*$^{-/-}$ South Hampshires, were randomised into treatment groups for this study (Table 1).

2.2. Vectors

Recombinant self-complementary AAV9 constructs, expressing codon-optimised ovine *CLN5* or *CLN6* (GenBank accession numbers NM_001082595 and NM_001040289 respectively) under the control of the CBh promoter (scAAV9.CLN5 and scAAV9.CLN6), were produced by the University of North Carolina Gene Therapy Center Vector Core (NC, USA) by triple transfection of HEK293 cells, iodixanol gradient centrifugation and ion-exchange chromatography as described (Grieger et al., 2016). Vectors were formulated in 350 mM phosphate buffered saline (PBS) containing 5% sorbitol, and titres determined by quantitative PCR (Grieger et al., 2016).

2.3. Ocular injections

The surgical procedure was performed by Stephen Heap (Veterinary Ophthalmologist, McMaster and Heap Veterinary Practice, Christchurch, NZ), based on methods previously established in dogs (Gearhart et al., 2010). Sheep were sedated by intravenous injection of 0.5 mg/kg live weight diazepam (Ilium, Troy Laboratories NZ Pty Ltd, Auckland, NZ) and 10 mg/kg live weight ketamine (Phoenix Ketamine injection, Phoenix Pharm Distributors Ltd, Auckland, NZ) prior to endotracheal intubation and maintenance on inhalation anaesthesia (isoflurane in oxygen, 1.5–3% v/v to effect). Sheep were placed in lateral recumbency on their right side. The surface of the left eye was prepared using 10% povidone-iodine solution (Betadine®, Avrio Health L.P., Stamford, CT, USA). The bulbar conjunctiva on the dorsolateral aspect of the eye was grasped with forceps, and the eye globe was rotated ventro-medially. The vector solution was injected using a 28-gauge ½ inch needle, inserted approximately 7 mm posterior to the sclera on the lateral aspect of the eye. The needle was angled posteriorly to avoid the lens, and the material was injected as close to the retina as possible without disturbing the retinal surface. Sheep received a single injection of 100 μl of scAAV9.CLN5 or scAAV9.CLN6 respectively into their left eye, at a total dose of 4×10^{11} viral genomes. Their right eye served as an internal control and was not treated. Following surgery, the animals were administered 0.5% chloramphenicol eye drops (Chlorafast, Teva Pharma Ltd, Auckland, NZ) 2–3 times daily for 7 days. Eye health, behaviour and rectal temperatures were monitored daily for 3 weeks post-surgery. Long term clinical monitoring included body weight, body condition, and general observation of abilities in the field.

2.4. Electroretinography

Electroretinography was conducted monthly using an Eickemeyer Veterinary ERG system (Eickemeyer - Medizintechnik für Tierärzte KG, Tuttlingen, Germany) as described previously (Russell et al., 2021). Pupils were dilated prior to recordings by the administration of 1% Tropicamide eyes drops (Mydriacyl®, 10 mg/mL; Alson NZ Ltd, Auckland, NZ). Sheep were anaesthetised via intravenous injection of diazepam (0.5 mg/kg live weight) and ketamine hydrochloride (10 mg/kg

Table 1
Sheep used in the current study.

Animal ID	Genotype	Sex	Treatment	Treatment age (months)	Delivery route	Dose (viral genomes)	Age at death (months)
1146/17	CLN5$^{-/-}$	E	scAAV9.CLN5	3	Intravitreal	4×10^{11}	18.3
1147/17	CLN5$^{-/-}$	E	scAAV9.CLN5	3	Intravitreal	4×10^{11}	18.3
1149/17	CLN5$^{-/-}$	E	scAAV9.CLN5	3	Intravitreal	4×10^{11}	18.3
1010/17	CLN6$^{-/-}$	E	scAAV9.CLN6	3	Intravitreal	4×10^{11}	18.2
1040/17	CLN6$^{-/-}$	E	scAAV9.CLN6	3	Intravitreal	4×10^{11}	18.4
1045/17	CLN6$^{-/-}$	E	scAAV9.CLN6	3	Intravitreal	4×10^{11}	18.4

E: Ewe, scAAV9: self-complementary AAV9 vector.

live weight), intubated, and maintained on inhalation anaesthesia (isoflurane in oxygen, 1.5–3% v/v to effect) for the duration of the procedure. The eye was kept open with a 40 mm Barraquer speculum, whilst an ERG-Jet contact lens recording electrode (Fabrinal SA, La Chaux-De-Fonds, Switzerland), primed with sterile saline solution, was placed on the eye. One subdermal 29-gauge ½ inch reference electrode (LKC Technologies Inc., Gaithersburg, MD, USA) was placed approximately 1 cm lateral to the lateral canthus, and a second subdermal ground electrode was placed on the dorsal surface of the skull 1 cm lateral to the midline in the direction of the eye being measured. The light stimulus was placed within 1 cm of the eye, and delivered 2–3 cd/m^2 white light four times consecutively with a 0.8 s delay. Measurements were made following 5 min of dark adaptation. Sheep were administered lubricating eye drops (POLY-TEARS®), at the conclusion of each recording session. The order of assessment of the treated and untreated eye was determined randomly between animals and between timepoints.

2.5. Histology

Sheep were sacrificed by penetrating captive bolt to the cervical spine followed by rapid exsanguination at approximately 18 months of age (Table 1). Eye globes were enucleated at the time of death, fixed in 10% formalin, approximately 2 h, and sent to Gribbles Veterinary Pathology, Christchurch, NZ for post-fixation in Bouin's solution (Sigma-Aldrich, St Louis, MO, USA, HT10132), 4 h, followed by wax embedding. Retinal paraffin sections were cut at 3 μm, mounted and a subset stained with Hematoxylin and Eosin (H + E) histological stain by Gribbles Veterinary Pathology for analysis of retinal thickness and layer differentiation. Brains were also collected at the time of death and processed for histology as previously described (Oswald et al., 2005).

2.6. Immunohistochemistry

Retinal paraffin sections were stained with either the inflammatory marker rabbit anti-cow glial fibrillary acidic protein (GFAP) or lysosome-associated membrane protein 1 (LAMP1). Sections were dewaxed twice in xylene (5 min) and rehydrated through a graded ethanol series to water. Following re-hydration sections underwent antigen retrieval in 10 mM Sodium Citrate buffer (pH 6) at 90 °C for 30 min, then allowed to cool for 20 min. Sections were then washed in TBST (Tris-buffered saline, pH 7.6, containing 0.3% Triton X-100) and blocked in 10% Normal Goat Serum (NGS) in TBST for 30 min at room temperature, before overnight incubation in the primary antibody (GFAP; 1:2500, Dako Z0334, Glostrup, Denmark; LAMP1; 1:500; Abcam ab24170, Cambridge, UK) in 10% NGS in TBST at 4 °C. Sections were washed in TBST and then incubated in goat anti-rabbit Alexa Fluor® 594 secondary antibody (1:500; Invitrogen A-11012, Carlsbad, CA, USA) 10% NGS in TBST, 1 h, in the dark at room temperature. Sections were then washed and incubated in DNA stain DAPI (4′,6-diamidino-2-phenylindole dihydrochloride; Sigma 10236276001) for 3 min at room temperature. DAPI was washed off in dH_20 and sections were coverslipped in BrightMount plus anti-fade mounting medium (Abcam ab103748).

A subset of unstained retinal paraffin sections and sagittal sheep brain sections were coverslipped in glycerol to assess autofluorescent storage body accumulation. Adjacent brain sections were stained with a standard cresyl violet Nissl stain as previous (Oswald et al., 2005), to detect cortical thickness and neuronal cytoarchitecture. Detection of CLN5 and CLN6 transduced cells in the sheep brain was performed with respective sheep-specific antibodies (1:500, R19122 and R19121ViraQuest, North Liberty, IA, USA) as previous (Mitchell et al., 2018). Brain and retinal sections from historical 18-month-old healthy control (n = 2–4) and affected (n = 2–4) animals were included in all histological procedures and analyses.

2.7. Image analysis

All H + E stained and unstained retinal sections were imaged on a Nikon Eclipse 50i microscope (Nikon Instruments Inc., Tokyo, Japan) paired to a Nikon Digital Sight DS-U3 camera and NIS-Elements BR software (v. 4.50 Nikon Instruments). Ten total retinal thickness measurements per eye were taken from the surface of the nerve fibre layer (NFL) to the base of the RPE in both the central retina (within 5 mm of the optic nerve head) and the peripheral retina (10–20 mm from the optic nerve head). Individual retinal layer thicknesses were then calculated from ten measurements per eye taken from the central retina. Autofluorescent lysosomal storage was imaged using a GFP Brightline® 490 excitation/510 emission filter set (GFP-3035C; Semrock Inc, IDEX Corporation, IL, USA). Ten images from the central retina were collected for each eye and thresholding analysis on ImageJ (NIH, version 1.52P) was used to determine the percentage of fluorescence per sampled area. The RPE and photoreceptor layers were excluded from thresholding analysis due to the endogenous fluorescence present in these cellular layers in the healthy control sheep eye.

Twenty-five cortical thickness measurements were taken through the primary visual cortex on Nissl stained brain sections as previously described (Oswald et al., 2005).

Immunofluorescent images were captured on a Zeiss 510 laser scanning confocal microscope with Zen 2009 imaging software (Carl Zeiss Microscopy). Image collection parameters (laser power, scan speed, pixel dwell time, detector gain, and pinhole size) were optimised for each channel and remained consistent for all sections in each staining run. High magnification Z-stacks were captured using a 40x/NA 1.3 oil objective and post-processing was performed in ImageJ.

2.8. Statistics

All statistical analysis was performed on GraphPad Prism© (v 8.2.0, GraphPad Software).

ERG amplitudes were calculated by the provided software (Eickemeyer). Animals were grouped by treatment and the repeated measurements were allocated into age-groups. Due to some missing data points a two-way repeated measures ANOVA was unable to be performed, therefore a mixed-effects model, fit using Restricted Maximum Likelihood (REML), was performed with Tukey's multiple comparisons test for each set of measurements to investigate the effects of time and treatment on the dark-adapted b-wave amplitude.

ERGs were also compared between groups and over time using Bayesian regression models, fitted to the "brms" (v2.13.5) package in R studio (v1.3.1056) (Bürkner, 2017). For each experimental group, ERG was modelled independently as a function of age, treatment, and age-by-treatment interaction, with a varying intercept and slope for each sheep; four chains with 2000 iterations each were used to generate posterior samples. Parameter estimates and 95% credible intervals are presented.

For histological analyses, results were reported as mean ± the standard error of the mean (SEM). Differences between the treated eye, untreated eye, and healthy and affected controls were assessed using a one-way ANOVA with Tukey's multiple comparisons test. Where homoscedasticity was not assumed, Brown-Forsythe and Welch ANOVA tests were performed with Dunnett's T3 multiple comparisons test to assess between group differences. Differences were regarded significant where the multiplicity adjusted p-value was < 0.05.

3. Results

3.1. Safety

The intravitreal treatment was well tolerated. One sheep (1149/17) developed posterior uveitis one-week post-injection, however this resolved within a week following three-time daily treatment with 0.5%

chloramphenicol eye drops (Chlorafast).

Observations of intravitreal treated sheep in the field demonstrated that they suffered clinical decline in line with affected controls; namely reduced herding, head tilt, low head carriage, crouching and baulking when moving through gates, difficulty navigating stairs, ataxia, and loss of body condition.

3.1.1. Ocular gene therapy in CLN5$^{-/-}$ sheep

Data from Russell et al. (2021) have shown that the earliest significant divergence between healthy control and CLN5 affected sheep was achieved at 11 months of age from ERG recordings taken following 5 min of dark adaptation. The b-wave amplitude (from the trough of the a-wave to the peak of the b-wave) was found to be the best and earliest predictor of retinal dysfunction (Russell et al., 2021). Hence results presented here use these same parameters.

Healthy control animals had relatively stable ERG amplitudes from 3- to 19-months of age, with an average rate of decline of −2.55 μV/month, which was not significantly different from a rate of decline of zero (Table 2). The ERG amplitudes of affected animals were visually distinguishable as lower than those from controls at 7 months and were significantly reduced from 11 months onwards, with an average rate of decline of −13 μV/month (Fig. 1A, Table 2).

In the ocular gene therapy animals, b-wave amplitudes declined steadily over time in the untreated eyes, at a rate of approximately 12.5 μV/month (Fig. 1A, Table 2). In contrast, average amplitude in the scAAV9.CLN5 treated eyes increased until 9 months of age and then subsequently stabilised. The treated eyes showed a rate of decline of 1.39 μV/month, and this was not significantly different from zero (Fig. 1A, Table 2). At 18 months of age, the average amplitude of the treated eyes (220 ± 45 μV) was double that of the untreated eyes (106 ± 15 μV), and comparable to ERG amplitudes of healthy controls of a similar age (Fig. 1A). At 5 months of age raw ERG traces look similar between the treated and untreated eye, however by 17 months of age there was little change in the treated ERG trace whilst the untreated trace was reduced (Fig. 1B). Whilst it is not evident in the representative image, there was a clear reduction in the a-wave amplitudes of the untreated eyes, which on average halved between 5 and 17 months of age, at a similar rate of decline to CLN5 affected sheep (Table S1). Yet there was no apparent loss in a-wave amplitude in the treated eyes.

Treated sheep were humanely euthanized with advanced clinical disease following their 18-month recording as a result of not receiving a brain-directed treatment. Eye globes and brains were processed for comparative histological analyses.

Total thickness measurements showed that the treated retina was significantly larger than the untreated retina in both the central (164 ± 2 μm vs 115 ± 2 μm, $p < 0.0001$) and peripheral (149 ± 6 μm vs 84 ± 2 μm, $p < 0.0001$) regions (Fig 2E, J). Individual layer thickness measurements in the central retina revealed that all layers except the RPE were significantly thicker in the treated eye compared to the untreated eye (Fig. 2K). The number of rows of photoreceptor nuclei was also quantified as a more precise measure of ONL thickness. Healthy control retina had on average 11 rows of photoreceptor nuclei in the ONL, while CLN5 affected retina had only 2 (Fig 2L). Consistent with the a-wave amplitude data (Table S1), untreated retina had comparable numbers of ONL rows to CLN5 affected retina, whereas treated eyes had significantly higher numbers compared with untreated (Fig 2L).

The presence and extent of lysosomal storage in the retina was assessed by confocal and epifluorescent microscopy. Co-localisation of

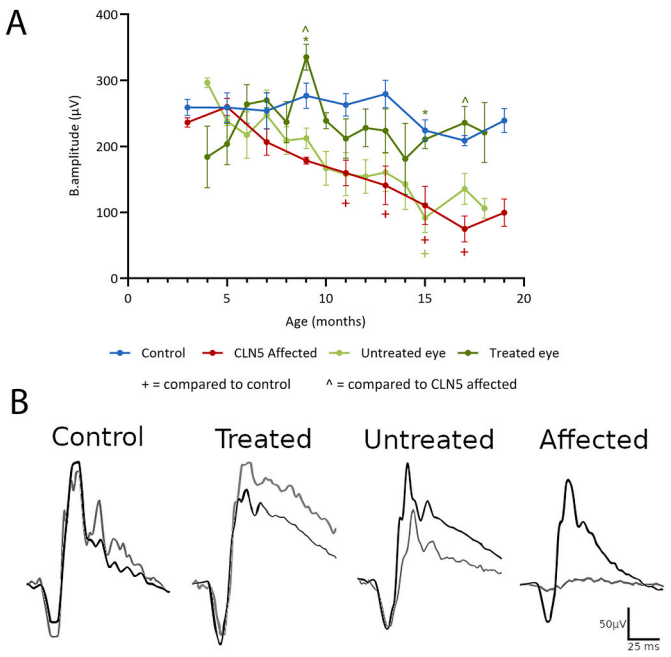

Fig. 1. Dark adapted ERG responses of CLN5$^{-/-}$ sheep following intravitreal delivery of AAV9.CLN5. (A) Mean (±SEM) ERG amplitudes over time in the treated (dark green, n = 3) and untreated (light green, n = 3) eye, and healthy control (blue, n = 6) and CLN5 affected (red, n = 6) sheep. (B) Representative ERG traces from the treated and untreated eyes, and controls at 5 (black line) and 17 (grey line) months of age. * indicates $P < 0.05$. (For interpretation of the references to colour in this figure legend, the reader is referred to the Web version of this article.)

autofluorescent signal with the lysosomal marker LAMP1 was imaged in the central retina (Fig. 3). In both the healthy control eyes and treated eyes there was minimal autofluorescent signal in the retina (0.60% and 0.56% fluorescence per area respectively), with any signal present coming from the IS/OS (Fig. 3A and B). In contrast, the CLN5 affected retina, along with the untreated retina, had significantly greater levels of autofluorescent signal across the retinal layers (2.6% and 1.3% fluorescence per area respectively) (Fig. 3C, D, Fig. S1). This was particularly evident as large puncta in the GCL which co-localised with LAMP1 and/or DAPI, indicating the presence of stereotypical intracellular lysosomal storage bodies in untreated retina.

Glial fibrillary acidic protein (GFAP) is an established immunohistochemical marker of retinal glial cells. Under normal conditions it is expressed in astrocytes in the NFL however retinal Müller cells will express GFAP during retinal stress. GFAP immunoreactivity was assessed in the central retina of treated and untreated eye compared to controls (Fig. 4). Treated eyes had low levels of GFAP immunoreactivity restricted to the NFL, which was comparable to healthy control eyes. While there was widespread GFAP-positive cells across the retina of CLN5 affected sheep, in untreated eyes immunoreactivity was primarily restricted to the NFL, albeit at higher levels compared to treated eyes.

The brain weights and primary visual cortex thickness in animals that received CLN5 ocular gene therapy were compared to historical healthy and CLN5 affected controls (Fig. 5). Brain weights for the treated sheep ranged from 63.7 to 65.8 g, significantly less than healthy controls

Table 2
Bayesian regression model comparing rate of decline in ERG responses between the control, affected, treated, and untreated eyes in CLN5 sheep.

	Control	Treated eye	Untreated eye	CLN5 affected
Slope (μV/month)	−2.55 *[-6.35, 1.23]*	−1.39 [*-5.2, 2.3*]	−12.55 [*-16.45, -8.9*]	−13.01 *[-16.3, -9.67]*

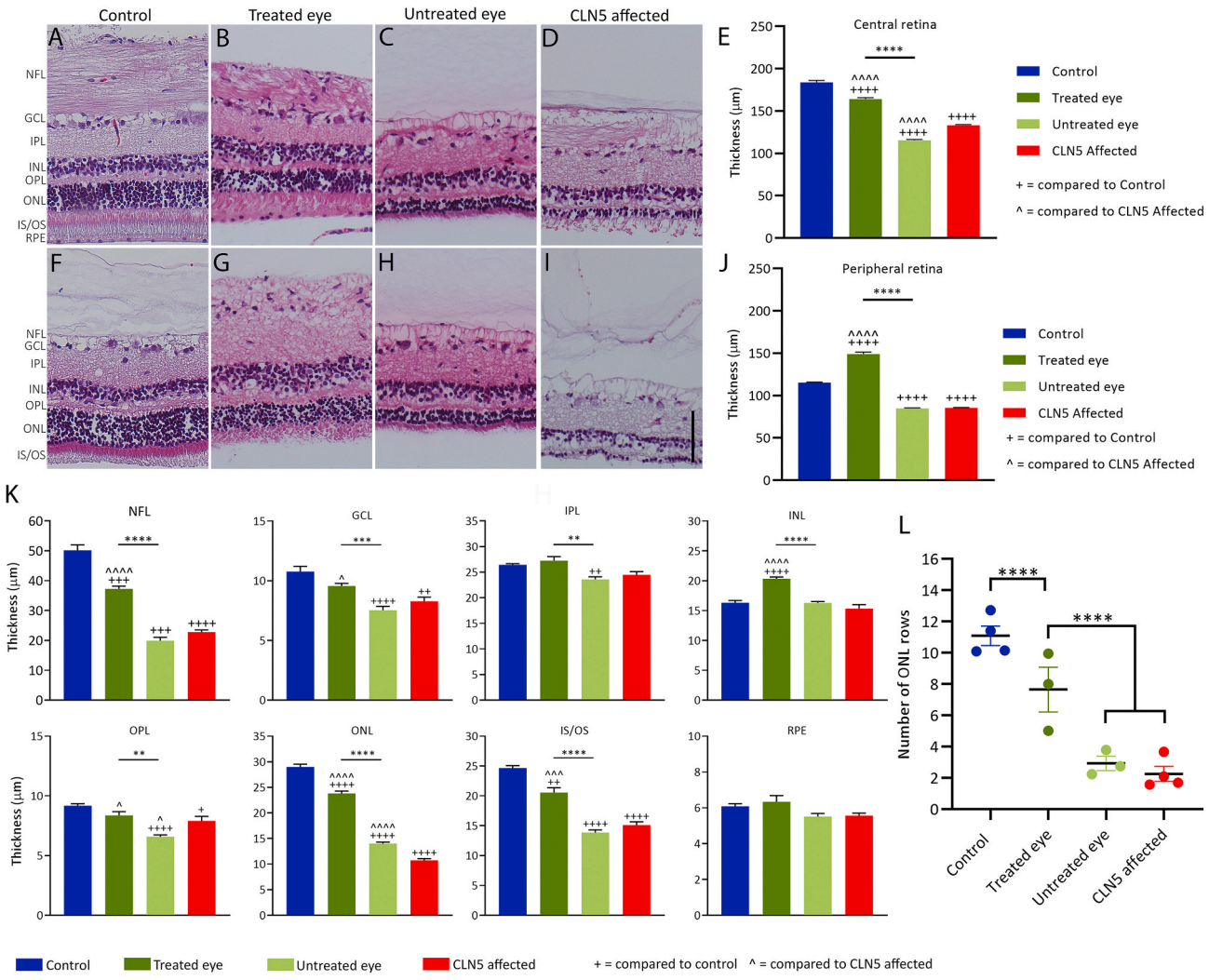

Fig. 2. Retinal thickness of CLN5$^{-/-}$ sheep following intravitreal delivery of AAV9.CLN5. Representative photomicrographs of H + E histological staining in the treated and untreated eyes compared to age-matched controls. Images and thickness measurements were taken in two locations; central retina (A–E) and peripheral retina (F–J). (E) Mean (±SEM) retinal thickness (μm) in the central retina of the treated (dark green, n = 3) and untreated (light green, n = 3) eyes compared with healthy (blue, n = 4) and CLN5 affected (red, n = 4) retina. (J) Mean (±SEM) retinal thickness (μm) in the peripheral retina of the treated and untreated eyes compared with healthy and CLN5 affected control retina. (K) The thickness of each retinal layer was measured in the central retina of treated (n = 3) and untreated (n = 3) eyes, and in eyes from healthy (n = 4) and CLN5 affected (n = 4) controls. * indicates $P < 0.05$, **** indicates $P < 0.0001$. NFL; nerve fibre layer, GCL; ganglion cell layer, IPL; inner plexiform layer, INL; inner nuclear layer, OPL; outer plexiform layer. ONL; outer nuclear layer, IS/OS; inner and outer segments of photoreceptors, RPE; retinal pigment epithelium. Scale bar 50 μm. (For interpretation of the references to colour in this figure legend, the reader is referred to the Web version of this article.)

(98.1 ± 1.1 g, n = 16) but in line with CLN5 affected controls (71.2 ± 1.5 g; n = 13). Similarly, there was significant atrophy of the visual cortex in treated sheep compared with healthy controls, and similar to CLN5 affected controls (Fig. 5). Immunostaining for CLN5 was carried out as previously described (Mitchell et al., 2018), however no CLN5-positive cells were detected across the brain indicating a lack of viral transduction in the brain following IVT delivery of scAAV9.CLN5. Assessment of autofluorescent signal in the lateral geniculate nucleus and primary visual cortex of treated animals was comparable between hemispheres and to age-matched CLN5 affected sheep (data not shown).

3.1.2. *Ocular gene therapy in CLN6$^{-/-}$ sheep*

As in CLN5 sheep, the b-wave amplitude following 5 min of dark adaptation was found to be the best and earliest predictor of retinal dysfunction in CLN6 sheep (Russell et al., 2021). Hence results presented here are the 5-min data adapted b-wave amplitudes.

Healthy control animals had stable ERG amplitudes from 3- to 19-months of age, with an average rate of decline of 0.44 μV/month, which was not significantly different from a rate of decline of zero (Table 3). The ERG amplitudes of affected animals rapidly declined from 3 months of age and were significantly reduced from 11 months onwards, with an average rate of decline of −14.4 μV/month (Fig. 6A, Table 3). By 17 months of age ERG amplitudes of affected animals were essentially extinguished, with an average amplitude of 14 ± 8 μV, compared to 211 ± 17 μV in control animals (Fig. 6A).

In the ocular gene therapy animals, there was a general trend of reduction in both a-wave and b-wave amplitudes in both treated and untreated eyes (Fig. 6A, Table S1). Whilst the rate of decline in b-wave amplitude of the treated eye (−8.5 μV/month) was smaller than the rate decline of the untreated eye (−14.0 μV/month), this difference was not significant (Table 3). At 17 months of age there was no difference in the average ERG amplitude between the treated (109 ± 46 μV) and untreated (110 ± 41 μV) eyes (Fig. 6A). At 5 and 17 months of age raw ERG traces look similar between the treated and untreated eye (Fig. 6B).

Total retinal thickness in the treated eye was significantly higher than the untreated eye in both the central and peripheral retina (Fig 7E,

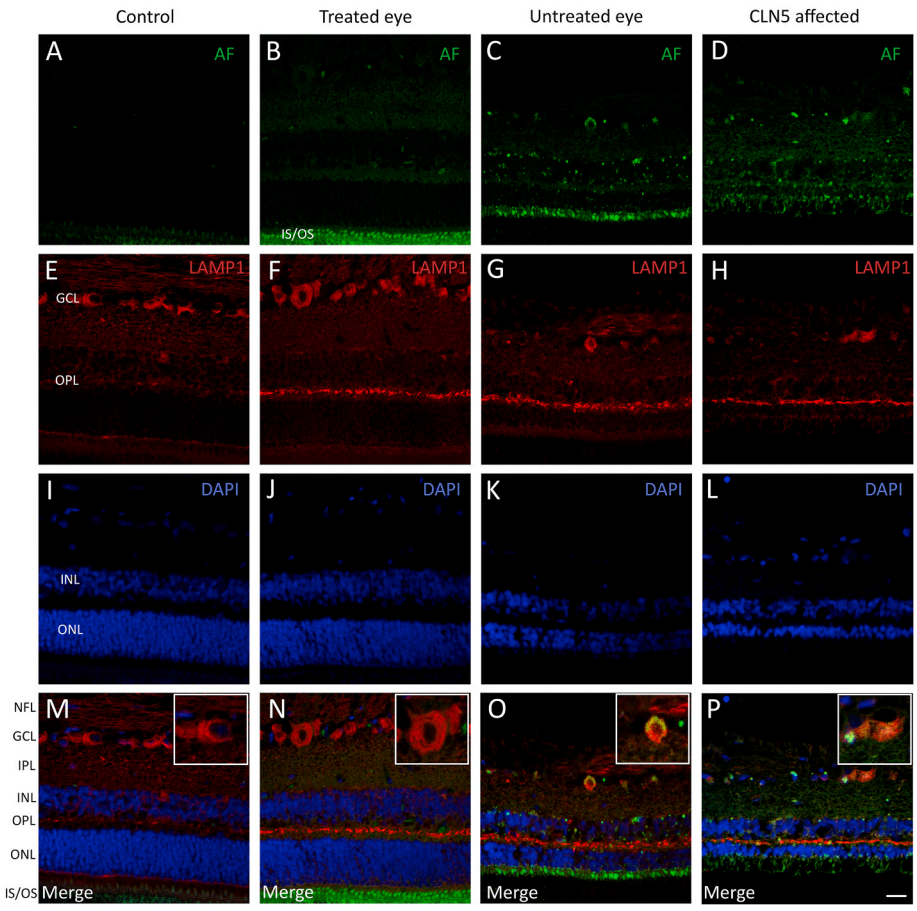

Fig. 3. Lysosomal storage in CLN5 affected sheep retina following intravitreal delivery of AAV9.CLN5. Representative images of co-localisation of autofluorescent signal with lysosomal marker LAMP1 was assessed in the treated and untreated retina compared to healthy and CLN5 affected controls. (A–D) Autofluorescent (AF) signal, (E–H) LAMP1 immunoreactivity, (I–L) DAPI nuclear stain, (M–P) Merged image of the 3 channels. Insets in O and P show zoomed images of co-localisation of AF and LAMP1 in cells in the GCL. NFL; nerve fibre layer, GCL; ganglion cell layer, IPL; inner plexiform layer, INL; inner nuclear layer, OPL; outer plexiform layer. ONL; outer nuclear layer, IS/OS; inner and outer segments of photoreceptors, Scale bar 20 μm.

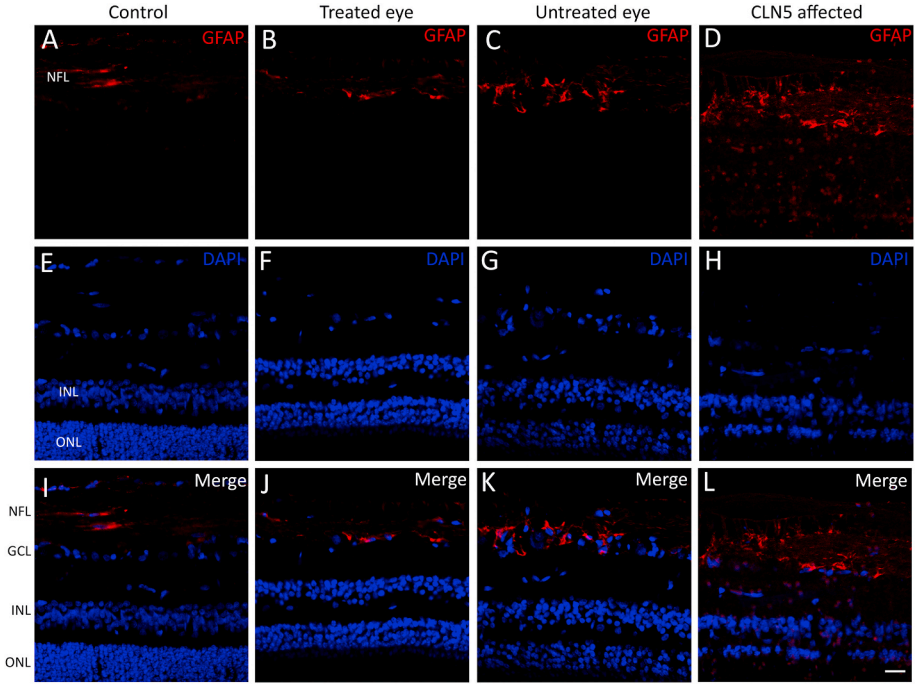

Fig. 4. GFAP immunoreactivity in the retina of CLN5$^{-/-}$ sheep following intravitreal delivery of AAV9.CLN5. Representative confocal images of GFAP immunoreactivity in the treated and untreated eyes compared to controls. (A–D) GFAP immunoreactivity, (E–H) DAPI nuclear marker, (I–L) Merged images of the 2 channels. NFL; nerve fibre layer, GCL; ganglion cell layer, INL; inner nuclear layer, ONL; outer nuclear layer, IS/OS; inner and outer segments of photoreceptors, Scale bar 20 μm.

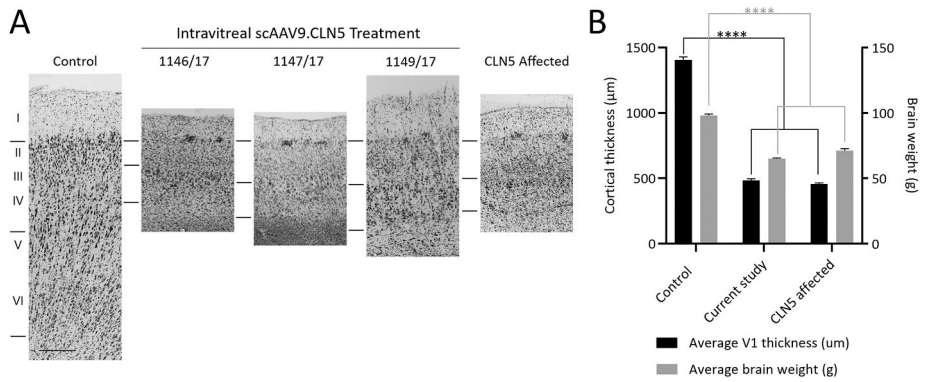

Fig. 5. Brain weight and primary visual cortex thickness following intravitreal delivery of AAV9.CLN5. (A) Representative photomicrographs of the primary visual cortex in IVT treated sheep and controls. (B) Average brain weight (grey, right y-axis) and average primary visual cortex thickness (black, left y-axis) in IVT treated sheep (current study) and controls. ****$P < 0.0001$.

Table 3
Bayesian regression model comparing rate of decline in ERG responses between the control, affected, treated, and untreated eyes in CLN6 sheep.

	Control	Treated eye	Untreated eye	CLN5 affected
Slope (µV/month)	0.44 *[-4.1, 4.5]*	−8.51 [*-13.5, -3.6*]	−14.0 [*-19.1, -8.7*]	−14.4 *[-18.9, -9.9]*

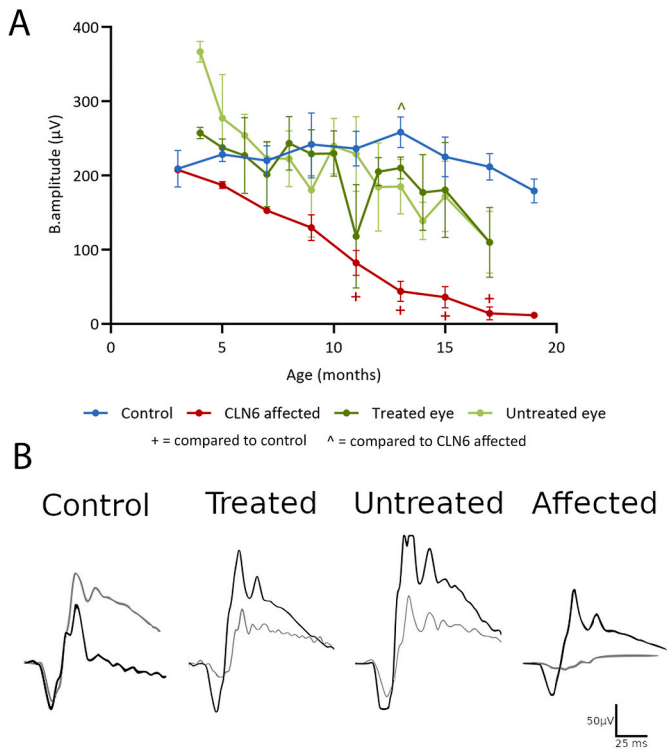

Fig. 6. Dark adapted ERG responses in CLN6$^{-/-}$ sheep following intravitreal delivery of AAV9.CLN6. (A) Mean (±SEM) ERG amplitudes over time in the treated (dark green, n = 3) and untreated (light green, n = 3) eye, and healthy control (blue, n = 6) and CLN6 affected (red, n = 6) sheep. (B) Representative ERG traces from the treated and untreated eyes, and controls at 5 (black line) and 17 (grey line) months of age. * indicates $P < 0.05$. (For interpretation of the references to colour in this figure legend, the reader is referred to the Web version of this article.)

J). Individual layer thickness measurements revealed significant atrophy of the NFL, GCL, outer plexiform layer (OPL), and ONL in the untreated eye compared to the treated eye (Fig. 7K). The inner and outer photoreceptor segments (IS/OS) layer showed significant atrophy in both the treated and untreated eyes at comparable levels to CLN6 affected retina. This was confirmed by ONL row counts of approximately 10 rows of nuclei in the healthy control retina but only 2–4 rows in the treated, untreated, and CLN6 affected retina (Fig 7L). This significant loss of photoreceptors seen on post-mortem correlated well with the reduction in a-wave amplitude evident at late stage disease (Table S1).

Healthy control retina had low levels of endogenous autofluorescent signal, again primarily confined to the IS/OS (Fig. 8A). Although there was no significant difference in the percentage of fluorescence between the treated retina and the healthy control (1.14% versus 0.67% fluorescence per area, Fig. S1), LAMP1 staining demonstrated the autofluorescent puncta in the GCL of the treated retina to be localised to the lysosome (Fig. 8B). However, significantly more lysosomal burden was evident in the ganglion cells of the untreated retina (2.4%), at levels comparable to a CLN6 affected retina (2.37% fluorescence per area).

GFAP immunoreactivity in the central retina was primarily confined to the NFL and comparable across treated, untreated, and CLN6 affected eyes (Fig. 9). Healthy control retina had little GFAP immunoreactivity.

The brain weights and primary visual cortex thickness in animals that received CLN6 ocular gene therapy were compared to historical healthy and CLN6 affected controls (Fig. 10). Mean brain weight for the treated sheep was 65.5 ± 1.1 g, significantly less than healthy controls (98.1 ± 1.1 g, n = 16) but in line with CLN6 affected controls (66.0 ± 2.4 g; n = 13). The thickness of the visual cortex in ocular gene therapy animals was significantly reduced compared to both healthy and CLN6 affected controls. Autofluorescent storage body accumulation was comparable to CLN6 affected controls and, whilst immunohistochemistry detected endogenous CLN6 protein in the healthy control brain, there were no transduced cells evident in the treated sheep brain (data not shown).

4. Discussion

This proof-of-concept study provides the first observation of efficacious intravitreal gene delivery in a large animal model of Batten

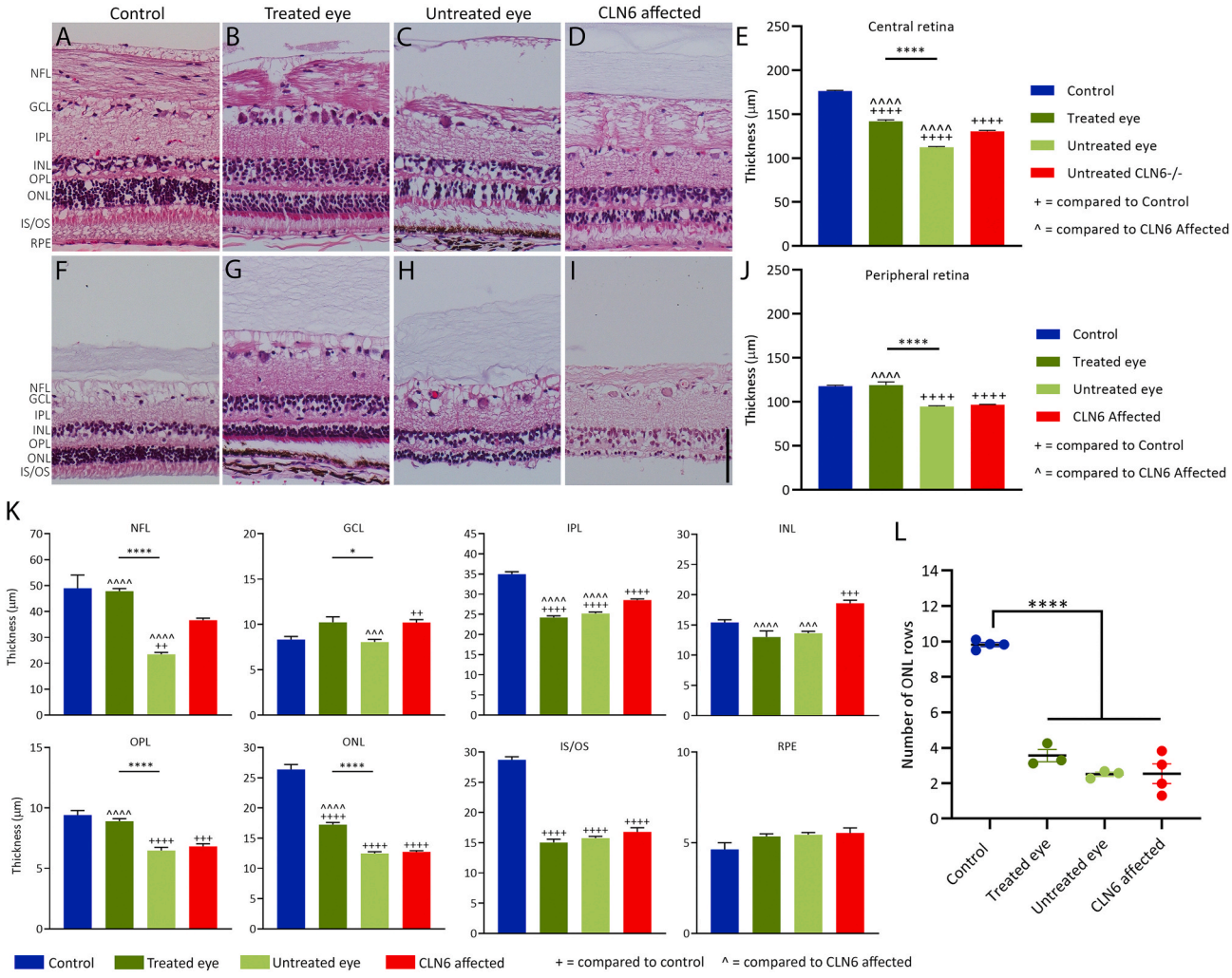

Fig. 7. Retinal thickness in CLN6 affected sheep following intravitreal delivery of AAV9.CLN6. Representative photomicrographs of H + E histological staining in the treated and untreated eyes compared to age-matched controls. Images and thickness measurements were taken in two locations; central retina (A–E) and peripheral retina (F–J). (E) Mean (±SEM) retinal thickness (μm) in the central retina of the treated (dark green, n = 3) and untreated (light green, n = 3) eyes compared with healthy (blue, n = 2) and CLN6 affected (red, n = 4) retina. (J) Mean (±SEM) retinal thickness (μm) in the peripheral retina of the treated and untreated eyes compared with healthy control and CLN6 affected retina. (K) The thickness of each retinal layer was measured in the central retina of treated (n = 3) and untreated (n = 3) eyes, and in eyes from healthy (n = 4) and CLN6 affected (n = 4) controls. * indicates $P < 0.05$, **** indicates $P < 0.0001$. NFL; nerve fibre layer, GCL; ganglion cell layer, IPL; inner plexiform layer, INL; inner nuclear layer, OPL; outer plexiform layer. ONL; outer nuclear layer, IS/OS; inner and outer segments of photoreceptors, RPE; retinal pigment epithelium. Scale bar 50 μm. (For interpretation of the references to colour in this figure legend, the reader is referred to the Web version of this article.)

disease. We have shown that a single administration of AAV9-mediated gene therapy to the vitreous of the eye can attenuate decline of retinal cell activity, retinal atrophy, and pathological storage body accumulation in sheep with naturally occurring CLN5 disease. Combining ocular gene therapy with brain-directed therapy presents a promising treatment strategy to be used in future sheep trials aiming to halt both the neurological and retinal disease, particularly in CLN5 disease.

Monthly assessment of retinal function using ERG showed near normalisation of function in the scAAV9.CLN5 treated eye, with a rate of decline comparable to that of healthy controls. In contrast, the untreated eye followed the typical decline of CLN5 affected sheep. Post-mortem histological analyses of the retina corroborated this finding, revealing significant degeneration and pathological lysosomal storage accumulation in the untreated retina, which had thicknesses comparable to that of an age-matched CLN5 affected controls. In contrast, the thickness of the CLN5 treated retina was comparable to age-matched healthy controls, with intact cellular/layer morphology and little lysosomal storage or inflammation.

As the scAAV9.CLN5 treated sheep did not receive any brain-directed treatment, they still developed stereotypical neurological disease and were humanely euthanized at approximately 18 months of age. Observations of these sheep in the field showed low head carriage, reduced herding and ultimately absent menace responses, indicative of vision loss. Post-mortem analyses revealed subnormal brain weights and significant atrophy of the primary visual cortex, similar to that reported for affected CLN5 sheep. This would suggest that although the treated retinal cells were still able to react to visual stimuli (e.g., ERG flashes of light), this information could not be processed by the damaged visual cortex, resulting in cortical blindness.

ERG amplitudes in the scAAV9.CLN6 treated eye of CLN6$^{-/-}$ animals were similar to the untreated eye, and while both were higher than CLN6 affected controls, they were not normalised to that of healthy control sheep. Post-mortem analyses showed minor attenuation of atrophy and lysosomal storage body accumulation in the retina of the CLN6 treated eye compared with the untreated eye but there was no therapeutic effect on the inflammatory response.

The sheep eye represents a good animal model of the human eye. It has an axial length of 26 mm, similar to the human eye (24 mm) while

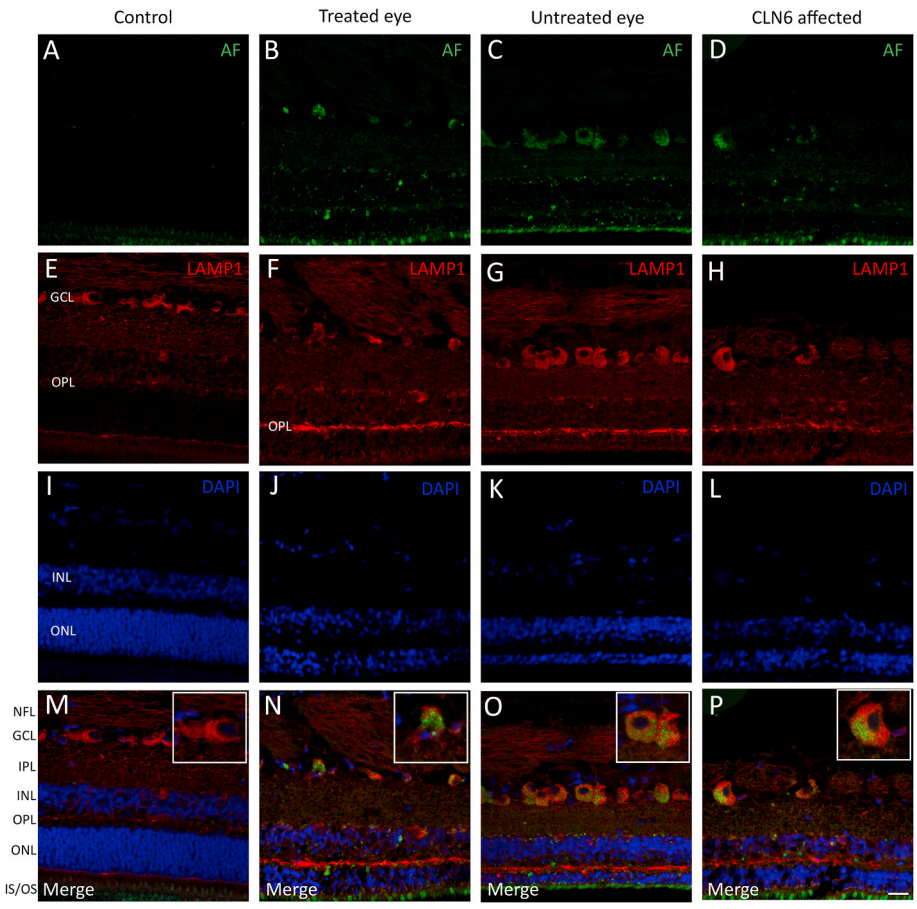

Fig. 8. Lysosomal storage in CLN6 affected sheep retina following intravitreal delivery of AAV9. CLN6. Representative images of co-localisation of autofluorescent signal with lysosomal marker LAMP1 was assessed in the treated and untreated retina compared to healthy and CLN6 affected controls. (A–D) Autofluorescent (AF) signal, (E–H) LAMP1 immunoreactivity, (I–L) DAPI nuclear stain, (M–P) Merged image of the 3 channels. Insets in O and P show zoomed images of co-localisation of AF and LAMP1 in cells in the GCL. NFL; nerve fibre layer, GCL; ganglion cell layer, IPL; inner plexiform layer, INL; inner nuclear layer, OPL; outer plexiform layer. ONL; outer nuclear layer, IS/OS; inner and outer segments of photoreceptors. Scale bar 20 μm.

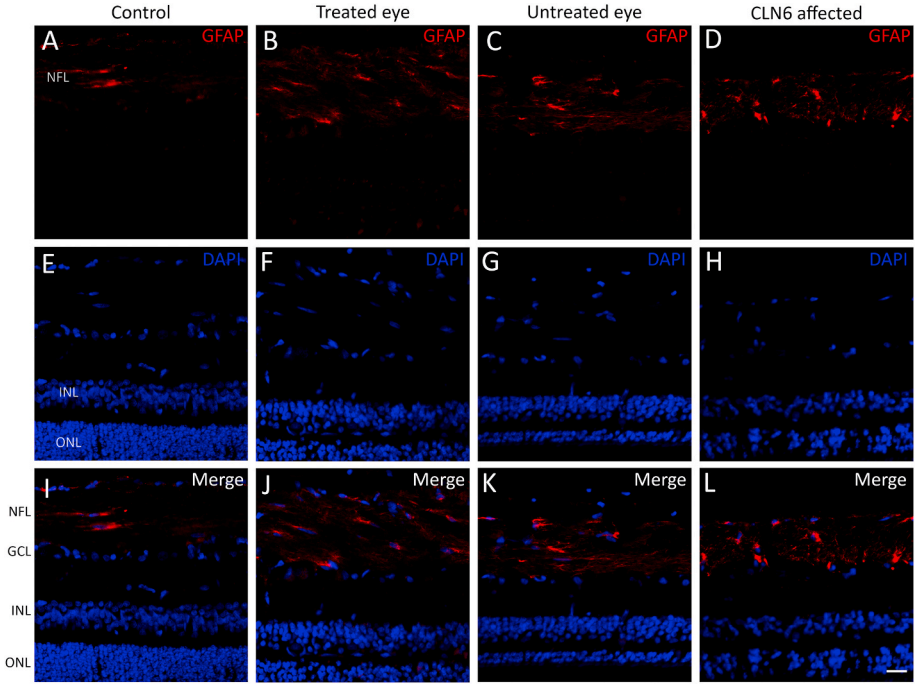

Fig. 9. GFAP immunoreactivity in the retina of CLN6 sheep following intravitreal delivery of AAV9.CLN6. Representative confocal images of GFAP immunoreactivity in the treated and untreated eyes compared to controls. (A–D) GFAP immunoreactivity, (E–H) DAPI nuclear marker, (I–L) Merged images of the 2 channels. NFL; nerve fibre layer, GCL; ganglion cell layer, INL; inner nuclear layer, ONL; outer nuclear layer, IS/OS; inner and outer segments of photoreceptors, Scale bar 20 μm.

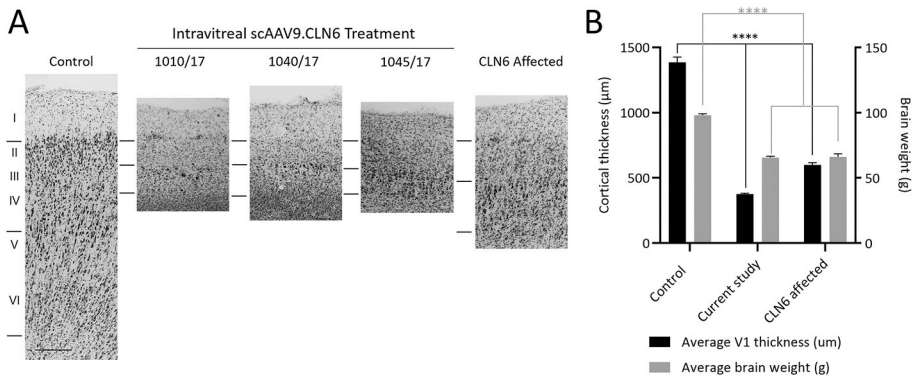

Fig. 10. Brain weight and primary visual cortex thickness following intravitreal delivery of AAV9.CLN6. Representative photomicrographs of the primary visual cortex in IVT treated sheep and controls. (B) Average brain weight (grey, right y-axis) and average primary visual cortex thickness (black, left y-axis) in IVT treated sheep (current study) and controls. ****$P < 0.0001$.

the rhesus macaque eye measures 18 mm (Howland et al., 2004; Yin et al., 2011). Adult sheep have a slightly larger vitreal volume (7 mL) when compared to the average human volume of 4.5 mL (Shafiee et al., 2008; Spitzer and Januschowski, 2015).Whilst the human eye has a circular pupil, sheep have a horizontally elongated oval shaped pupil, adapted to give them a wide visual field for detecting predators. They also possess a tapetum lucidum; a membranous layer of tissue sitting behind the retina which reflects light back to the retina, increasing photon capture by photoreceptors (Kostic and Arsenijevic, 2016). At the cellular level, the fundamental 10-layered morphology of the retina is very similar between sheep and humans, although sheep only possess two types of cone photoreceptors (M- and S-cones) whereas humans possess three types of cones (M-, S-, and L-cones) (Kostic and Arsenijevic, 2016; Shinozaki et al., 2010). Although the sheep retina does not have the macula or fovea of human eye, it has two similar cone-enriched regions instead: a streak in the central part of the retina (area centralis) and a smaller dorso-temporal area (Kostic and Arsenijevic, 2016; Shinozaki et al., 2010). These similarities in eye globe dimensions and retinal morphology are encouraging when considering the translational feasibility of ocular gene therapy between sheep and humans.

The eye is considered immune privileged due to the presence of the blood-retina barrier (BRB) formed by non-fenestrated capillaries and tight junctions in the RPE (Willett and Bennett, 2013). This combined with the low immunogenicity of adeno-associated viruses makes ocular gene therapy a promising method for treating diseases of the retina. Sub-retinal delivery is generally the preferred delivery route for treating diseases affecting the outer retina due to its direct targeting of PR and RPE cells. However, sub-retinal injections involve retinal detachment at the location of the bleb which should be temporary, but in some cases causes permanent structural damage such as a retinal tear or macular hole that is detrimental to visual processing (Dalkara et al, 2009, 2013). In degenerative diseases the retina is often more fragile and prone to detachment at the photoreceptor-RPE boundary which adds an additional element of risk to this delivery route. Conversely intravitreal delivery, although less specifically targeted, is much less invasive and poses a lower risk of physical trauma to the retina.

AAV vectors have emerged as the predominant vector for ocular gene therapy (Schön et al., 2015). The different AAV serotypes display varying affinities to particular cell types and have differing abilities to penetrate barriers, such as the inner limiting membrane (ILM) of the retina (Kiss, 2020). Several studies have attempted to increase transduction efficiency of AAV vectors by disrupting the ILM, primarily by protease-mediated digestion, saturation of ILM viral binding sites, or surgical ILM peeling. In sheep, pre-treatment with an unmodified, non-penetrating AAV2 vector was performed prior to capsid-modified AAV2 administration with the aim of saturating viral binding sites on the ILM and therefore increasing transduction (Ross et al., 2020). Unfortunately, this did not have the desired effect as no gene expression was detected in the target outer retinal cells. Surgical ILM peeling has produced mixed results in large animals (Boyd et al., 2016a; Takahashi et al., 2017) however digestion of the ILM by pre-treatment with non-specific proteases has shown promise in both small and large animals. In mice, co-injection of non-specific proteases with AAV vector resulted in robust transduction of AAV1, 2, 5, 8, and 9 throughout the retina (Dalkara et al., 2009), while in non-human primates protease pre-treatment increased AAV2 transduction and subsequent gene expression in the retina (Yin et al., 2011).

The current study utilised AAV9 as this was in use in similar brain-directed gene therapy studies in NCL sheep (Mitchell et al., 2018). If AAV9-mediated gene therapy was effective in both brain and retina, it would simplify dosing in clinical trials, as treatments could be given concurrently requiring only one procedure and exposure to only one AAV serotype. Whilst AAV9 is not typically the first choice for targeting retinal cells, and has not been tested in large animal eyes to date, it does bind to the ILM of the retina following intravitreal injections in rodents, and can produce gene expression in the inner retina when the ILM is disrupted (Dalkara et al., 2009). However, caution should be taken when translating positive results in the rodent eye to a larger animal eye, as evidenced by studies utilising capsid-modified AAV2 and AAV8 whereby the robust and moderate transduction observed in mouse and dog retina, respectively, was unable to be replicated in the sheep retina (Boyd et al., 2016b; Kay et al., 2013; Ross et al., 2020).

The results seen in the CLN5 sheep eye treated with AAV9.CLN5 in the current study were encouraging, yet further investigation is needed to elucidate the mechanism of action leading to this attenuation of retinal dysfunction and pathology. Unfortunately, localisation of CLN5 (and CLN6) proteins in the sheep retina has not been possible to date. Currently available antibodies against CLN5 and CLN6 work in central nervous system tissues but do not produce staining in either 5 µm paraffin embedded or 50 µm fixed retinal sections (data not shown), making it difficult to assess the number and types of cells transduced in the current study. In the human eye CLN5 expression is highest in Müller cells, the glial supporting cells of the retina, which fits with data showing high levels of CLN5 expression in glia in both the human and mouse brain (Holmberg et al., 2004; Schmiedt et al., 2012; Uhlen et al., 2010, v20.proteinatlas.org). In contrast, CLN6 expression is most highly expressed in human and mouse retinal bipolar cells (kleine Holthaus et al., 2018; Uhlén et al., 2015, v20.proteinatlas.org). The similarities in CLN5 and CLN6 expression profiles between human and mouse retina suggest similar profiles could be expected in the sheep retina, particularly given the high degree of homology between human, mouse, and sheep protein sequences (Frugier et al., 2008; Tammen et al., 2006). However, given the current challenges around localising and quantifying CLN5 and CLN6 immunoreactivity in the sheep retina, we plan to

administer AAV9.GFP intravitreally and assess the distribution of GFP to determine the transduction efficiency and cell specificity of AAV9 in the sheep retina.

The phenomenon of cross-correction likely accounts for the difference in efficacy between CLN5 and CLN6 animals (Sands and Davidson, 2006). Whilst the sheep ILM is not particularly well characterised, unmodified AAV2 vector has been shown bind to it resulting in gene expression in the inner retinal layers (Ross et al., 2020). This may mean that even if AAVs cannot penetrate to the outer retinal layers following intravitreal delivery, perhaps the functional protein secreted by transduced inner retinal cells can. CLN5 is a soluble protein, therefore only a subset of transduced cells producing the functional protein may be sufficient to rescue disease pathology and phenotype (Parenti et al., 2015). This has been demonstrated in ocular gene therapy studies in CLN1 mice, who are deficient in the soluble lysosomal enzyme, palmitoyl-protein thioesterase 1 (PPT1) (Griffey et al., 2005). Following intravitreal delivery of AAV2-PPT1 to affected mice, transduction of inner retinal cells was able to produce supra-physiological levels of PPT1 enzyme activity in the retina and improve retinal pathology. Although protein expression and improved pathology was detected in the brains of mice following intravitreal PPT1 delivery (Griffey et al., 2005), neither transduced cells nor attenuation of lysosomal storage were detected in the brain of CLN5 treated sheep in the current study, indicating that extra-ocular correction did not occur after intravitreal delivery to the sheep eye. In contrast to CLN5, CLN6 is a membrane bound protein localised to the endoplasmic reticulum therefore increasing retinal transduction by disrupting the ILM or using modified vectors is likely to be necessary to maximise therapeutic efficacy. Indeed, in mouse models of CLN3 and CLN6, bipolar cell-specific delivery of *CLN3* or *CLN6* protected the retina from dysfunction and cell death (Kleine Holthaus et al., 2020; kleine Holthaus et al., 2018), therefore a similar approach using cell-specific promotors should be considered for improving future intravitreal gene therapies in these sheep.

5. Conclusions

This pilot study provides proof-of-concept evidence of the efficacy of intravitreal gene therapy for the ocular changes associated with CLN5 Batten disease. A single administration of scAAV9.CLN5 into the eye of sheep with naturally occurring CLN5 disease was able to slow the deterioration of vision and attenuate retinal atrophy and accumulation of pathological storage material in the retina. Conversely, intravitreal delivery of scAAV9.CLN6 to CLN6 affected sheep did not prevent retinal dysfunction and pathology. This intravitreal approach is now being trialled in conjunction with brain-directed therapy on CLN5 sheep at various disease stages.

Declaration of competing interest

SJG received patent royalty income from Asklepios Biopharmaceutics for IP not used in this study, and also patent royalty income from Neurogene.

Acknowledgements

This work was supported by CureKids New Zealand, the Canterbury Medical Research Foundation (CMRF), Neurogene Inc. and the Batten Disease Support and Research Association (BDRSA).

Appendix A. Supplementary data

Supplementary data to this article can be found online at https://doi.org/10.1016/j.exer.2021.108600.

References

Boyd, R.F., Boye, S.L., Conlon, T.J., Erger, K.E., Sledge, D.G., Langohr, I.M., Hauswirth, W.W., Komáromy, A.M., Boye, S.E., Petersen-Jones, S.M., Bartoe, J.T., 2016a. Reduced retinal transduction and enhanced transgene-directed immunogenicity with intravitreal delivery of rAAV following posterior vitrectomy in dogs. Gene Ther. 23, 548–556. https://doi.org/10.1038/gt.2016.31.

Boyd, R.F., Sledge, D.G., Boye, S.L., Boye, S.E., Hauswirth, W.W., Komáromy, A.M., Petersen-Jones, S.M., Bartoe, J.T., 2016b. Photoreceptor-targeted gene delivery using intravitreally administered AAV vectors in dogs. Gene Ther. 23, 223–230. https://doi.org/10.1038/gt.2015.96.

Bürkner, P.-C., 2017. Brms: an R package for bayesian multilevel models using stan. J. Stat. Software 80, 1–28. https://doi.org/10.18637/jss.v080.i01.

Cooper, J.D., Tarczyluk, M.A., Nelvagal, H.R., 2015. Towards a new understanding of NCL pathogenesis. BBA-Mol. Basis. Dis. 1852, 2256–2261. https://doi.org/10.1016/j.bbadis.2015.05.014.

Dalkara, D., Byrne, L.C., Klimczak, R.R., Visel, M., Yin, L., Merigan, W.H., Flannery, J.G., Schaffer, D.V., 2013. In vivo–directed evolution of a new adeno-associated virus for therapeutic outer retinal gene delivery from the vitreous. Sci. Transl. Med. 5, 189ra76. https://doi.org/10.1126/scitranslmed.3005708, 189ra76.

Dalkara, D., Kolstad, K.D., Caporale, N., Visel, M., Klimczak, R.R., Schaffer, D.V., Flannery, J.G., 2009. Inner limiting membrane barriers to AAV-mediated retinal transduction from the vitreous. Mol. Ther. 17, 2096–2102. https://doi.org/10.1038/mt.2009.181.

Frugier, T., Mitchell, N.L., Tammen, I., Houweling, P.J., Arthur, D.G., Kay, G.W., van Diggelen, O.P., Jolly, R.D., Palmer, D.N., 2008. A new large animal model of CLN5 neuronal ceroid lipofuscinosis in Borderdale sheep is caused by a nucleotide substitution at a consensus splice site (c.571+1G>A) leading to excision of exon 3. Neurobiol. Dis. 29, 306–315. https://doi.org/10.1016/j.nbd.2007.09.006.

Gearhart, P.M., Gearhart, C., Thompson, D.A., Petersen-Jones, S.M., 2010. Improvement of visual performance with intravitreal administration of 9-cis-retinal in Rpe65-mutant dogs. Arch. Ophthalmol. 128, 1442–1448. https://doi.org/10.1001/archophthalmol.2010.210.

Goebel, H.H., Fix, J.D., Zeman, W., 1974. The fine structure of the retina in neuronal ceroid-lipofuscinosis. Am. J. Ophthalmol. 77, 25–39. https://doi.org/10.1016/0002-9394(74)90601-1.

Goebel, H.H., Köhnecke, B., Koppang, N., 1982. Ultrastructural studies on the retina in human and canine neuronal ceroid-lipofuscinoses and other lysosomal disorders. Birth Defects-Orig 18, 241–253.

Graydon, R.J., Jolly, R.D., 1984. Ceroid-lipofuscinosis (Batten's disease). Sequential electrophysiologic and pathologic changes in the retina of the ovine model. Invest. Ophthalmol. Vis. Sci. 25, 294–301.

Grieger, J.C., Soltys, S.M., Samulski, R.J., 2016. Production of recombinant adeno-associated virus vectors using suspension HEK293 cells and continuous harvest of vector from the culture media for GMP FIX and FLT1 clinical vector. Mol. Ther. 24, 287–297. https://doi.org/10.1038/mt.2015.187.

Griffey, M., Macauley, S.L., Ogilvie, J.M., Sands, M.S., 2005. AAV2-mediated ocular gene therapy for infantile neuronal ceroid lipofuscinosis. Mol. Ther. 12, 413–421. https://doi.org/10.1016/j.ymthe.2005.04.018.

Harden, A., Pampiglione, G., 1982. Neurophysiological studies (EEG/ERG/VEP/SEP) in 88 children with so-called neuronal ceroid lipofuscinosis. In: Armstrong, D., Koppang, N., Rider, J.A. (Eds.), Ceroid-Lipofuscinosis (Batten's Disease). Elsevier Biomedical Press, Amsterdam, pp. 61–70.

Holmberg, V., Jalanko, A., Isosomppi, J., Fabritius, A.-L., Peltonen, L., Kopra, O., 2004. The mouse ortholog of the neuronal ceroid lipofuscinosis CLN5 gene encodes a soluble lysosomal glycoprotein expressed in the developing brain. Neurobiol. Dis. 16, 29–40. https://doi.org/10.1016/j.nbd.2003.12.019.

Howland, H.C., Merola, S., Basarab, J.R., 2004. The allometry and scaling of the size of vertebrate eyes. Vis. Res. 44, 2043–2065. https://doi.org/10.1016/j.visres.2004.03.023.

Jolly, R., Arthur, D., Kay, G., Palmer, D., 2002. Neuronal ceroid-lipofuscinosis in Borderdale sheep. N. Z. Vet. J. 50, 199–202. https://doi.org/10.1080/00480169.2002.36311.

Jolly, R.D., Janmaat, A., Graydon, R.J., Clemett, R.S., 1982. Ceroid-Lipofuscinosis: the ovine model. In: Armstrong, D., Koppang, N., Rider, J.A. (Eds.), Ceroid-Lipofuscinosis (Batten's Disease). Elsevier Biomedical Press, Amsterdam, pp. 218–228.

Jolly, R.D., Shimada, A., Dopfmer, I., Slack, P.M., Birtles, M.J., Palmer, D.N., 1989. Ceroid–lipofuscinosis (batten's disease): pathogenesis and sequential neuropathological changes in the ovine model. Neuropathol. Appl. Neurobiol. 15, 371–383. https://doi.org/10.1111/j.1365-2990.1989.tb01236.x.

Jolly, R.D., West, D.M., 1976. Blindness in South Hampshire sheep: a neuronal ceroid lipofuscinosis. N. Z. Vet. J. 24, 123. https://doi.org/10.1080/00480169.1976.34298.

Katz, M.L., Tecedor, L., Chen, Y., Williamson, B.G., Lysenko, E., Wininger, F.A., Young, W.M., Johnson, G.C., Whiting, R.E.H., Coates, J.R., Davidson, B.L., 2015. AAV gene transfer delays disease onset in a TPP1-deficient canine model of the late infantile form of Batten disease. Sci. Transl. Med. 7, 180. https://doi.org/10.1126/scitranslmed.aac6191.

Kay, C.N., Ryals, R.C., Aslanidi, G.V., Min, S.H., Ruan, Q., Sun, J., Dyka, F.M., Kasuga, D., Ayala, A.E., Van Vliet, K., Agbandje-McKenna, M., Hauswirth, W.W., Boye, S.L., Boye, S.E., 2013. Targeting photoreceptors via intravitreal delivery using novel, capsid-mutated AAV vectors. PloS One 8, e62097. https://doi.org/10.1371/journal.pone.0062097.

Kiss, S., 2020. Vector Considerations for Ocular Gene Therapy. Adeno-associated virus vectors offer a safe and effective tool for gene delivery. Retin. Physician 40–45.

Kleine Holthaus, S.-M., Aristorena, M., Maswood, R., Semenyuk, O., Hoke, J., Hare, A., Smith, A.J., Mole, S.E., Ali, R.R., 2020. Gene therapy targeting the inner retina rescues the retinal phenotype in a mouse model of CLN3 batten disease. Hum. Gene Ther. 31, 709–718. https://doi.org/10.1089/hum.2020.038.

kleine Holthaus, S.-M., Ribeiro, J., Abelleira-Hervas, L., Pearson, R.A., Duran, Y., Georgiadis, A., Sampson, R.D., Rizzi, M., Hoke, J., Maswood, R., Azam, S., Luhmann, U.F.O., Smith, A.J., Mole, S.E., Ali, R.R., 2018. Prevention of photoreceptor cell loss in a Cln6 mouse model of batten disease requires CLN6 gene transfer to bipolar cells. Mol. Ther. 26, 1343–1353. https://doi.org/10.1016/j.ymthe.2018.02.027.

Kohlschütter, A., Schulz, A., Bartsch, U., Storch, S., 2019. Current and emerging treatment strategies for neuronal ceroid lipofuscinoses. CNS Drugs 33, 315–325. https://doi.org/10.1007/s40263-019-00620-8.

Kostic, C., Arsenijevic, Y., 2016. Animal modelling for inherited central vision loss. J. Pathol. 238, 300–310. https://doi.org/10.1002/path.4641.

Kousi, M., Lehesjoki, A.-E., Mole, S.E., 2012. Update of the mutation spectrum and clinical correlations of over 360 mutations in eight genes that underlie the neuronal ceroid lipofuscinoses. Hum. Mutat. 33, 42–63. https://doi.org/10.1002/humu.21624.

Mayhew, I.G., Jolly, R.D., Pickett, B.T., Slack, P.M., 1985. Ceroid-lipofuscinosis (Batten's disease): pathogenesis of blindness in the ovine model. Neuropathol. Appl. Neurobiol. 11, 273–290. https://doi.org/10.1111/j.1365-2990.1985.tb00025.x.

Mitchell, N.L., Russell, K.N., Wellby, M.P., Wicky, H.E., Schoderboeck, L., Barrell, G.K., Melzer, T.R., Gray, S.J., Hughes, S.M., Palmer, D.N., 2018. Longitudinal in vivo monitoring of the CNS demonstrates the efficacy of gene therapy in a sheep model of CLN5 batten disease. Mol. Ther. 26, 2366–2378. https://doi.org/10.1016/j.ymthe.2018.07.015.

Mole, S.E., Anderson, G., Band, H.A., Berkovic, S.F., Cooper, J.D., Holthaus, S.-M.K., McKay, T.R., Medina, D.L., Rahim, A.A., Schulz, A., Smith, A.J., 2019. Clinical challenges and future therapeutic approaches for neuronal ceroid lipofuscinosis. Lancet Neurol. 18, 107–116. https://doi.org/10.1016/S1474-4422(18)30368-5.

Mole, S.E., Cotman, S.L., 2015. Genetics of the neuronal ceroid lipofuscinoses (Batten disease). BBA-Mol. Basis. Dis., Current Research on the Neuronal Ceroid Lipofuscinoses (Batten Disease) 1852, 2237–2241. https://doi.org/10.1016/j.bbadis.2015.05.011.

Mole, S.E., Williams, R.E., Goebel, H.H., 2011. The Neuronal Ceroid Lipofuscinoses (Batten Disease), second ed. Oxford University Press.

Mole, S.E., Williams, R.E., Goebel, H.H., 2005. Correlations between genotype, ultrastructural morphology and clinical phenotype in the neuronal ceroid lipofuscinoses. Neurogenetics 6, 107–126. https://doi.org/10.1007/s10048-005-0218-3.

Oswald, M.J., Palmer, D.N., Kay, G.W., Shemilt, S.J., Rezaie, P., Cooper, J.D., 2005. Glial activation spreads from specific cerebral foci and precedes neurodegeneration in presymptomatic ovine neuronal ceroid lipofuscinosis (CLN6). Neurobiol. Dis. 20, 49–63. https://doi.org/10.1016/j.nbd.2005.01.025.

Parenti, G., Andria, G., Ballabio, A., 2015. Lysosomal storage diseases: from pathophysiology to therapy. Annu. Rev. Med. 66, 471–486. https://doi.org/10.1146/annurev-med-122313-085916.

Radke, J., Stenzel, W., Goebel, H.H., 2015. Human NCL neuropathology. Biochim. Biophys. Acta 1852, 2262–2266. https://doi.org/10.1016/j.bbadis.2015.05.007.

Rider, J.A., Rider, D.L., Opitz, J.M., Reynolds, J.F., Pullarkat, R.K., 1988. Batten disease: past, present, and future. Am. J. Med. Genet. 31, 21–26.

Ross, M., Obolensky, A., Averbukh, E., Ezra-Elia, R., Yamin, E., Honig, H., Dvir, H., Rosov, A., Hauswirth, W.W., Gootwine, E., Banin, E., Ofri, R., 2020. Evaluation of photoreceptor transduction efficacy of capsid-modified adeno-associated viral vectors following intravitreal and subretinal delivery in sheep. Hum. Gene Ther. 31, 719–729. https://doi.org/10.1089/hum.2020.023.

Russell, K.N., Mitchell, N.L., Wellby, M.P., Barrell, G.K., Palmer, D.N., 2021. Electroretinography data from ovine models of CLN5 and CLN6 neuronal ceroid lipofuscinoses. Data In Brief. Submitted for publication.

Sands, M.S., Davidson, B.L., 2006. Gene therapy for lysosomal storage diseases. Mol. Ther. 13, 839–849. https://doi.org/10.1016/j.ymthe.2006.01.006.

Schmiedt, M.-L., Blom, Tea, Blom, Tomas, Kopra, O., Wong, A., von Schantz-Fant, C., Ikonen, E., Kuronen, M., Jauhiainen, M., Cooper, J.D., Jalanko, A., 2012. Cln5-deficiency in mice leads to microglial activation, defective myelination and changes in lipid metabolism. Neurobiol. Dis. 46, 19–29. https://doi.org/10.1016/j.nbd.2011.12.009.

Schön, C., Biel, M., Michalakis, S., 2015. Retinal gene delivery by adeno-associated virus (AAV) vectors: strategies and applications. Eur. J. Pharm. Biopharm. 95, 343–352. https://doi.org/10.1016/j.ejpb.2015.01.009.

Shafiee, A., McIntire, G.L., Sidebotham, L.C., Ward, K.W., 2008. Experimental determination and allometric prediction of vitreous volume, and retina and lens weights in Göttingen minipigs. Vet. Ophthalmol. 11, 193–196. https://doi.org/10.1111/j.1463-5224.2008.00619.x.

Shinozaki, A., Hosaka, Y., Imagawa, T., Uehara, M., 2010. Topography of ganglion cells and photoreceptors in the sheep retina. J. Comp. Neurol. 518, 2305–2315. https://doi.org/10.1002/cne.22333.

Sondhi, D., Scott, E.C., Chen, A., Hackett, N.R., Wong, A.M.S., Kubiak, A., Nelvagal, H.R., Pearse, Y., Cotman, S.L., Cooper, J.D., Crystal, R.G., 2013. Partial correction of the CNS lysosomal storage defect in a mouse model of juvenile neuronal ceroid lipofuscinosis by neonatal CNS administration of an adeno-associated virus serotype rh.10 vector expressing the human CLN3 gene. Hum. Gene Ther. 25, 223–239. https://doi.org/10.1089/hum.2012.253.

Spitzer, M.S., Januschowski, K., 2015. [Aging and age-related changes of the vitreous body]. Ophthalmologe 112 (552), 554–558. https://doi.org/10.1007/s00347-015-0031-9.

Takahashi, K., Igarashi, T., Miyake, K., Kobayashi, M., Yaguchi, C., Iijima, O., Yamazaki, Y., Katakai, Y., Miyake, N., Kameya, S., Shimada, T., Takahashi, H., Okada, T., 2017. Improved intravitreal AAV-mediated inner retinal gene transduction after surgical internal limiting membrane peeling in cynomolgus monkeys. Mol. Ther. 25, 296–302. https://doi.org/10.1016/j.ymthe.2016.10.008.

Tammen, I., Houweling, P.J., Frugier, T., Mitchell, N.L., Kay, G.W., Cavanagh, J.A.L., Cook, R.W., Raadsma, H.W., Palmer, D.N., 2006. A missense mutation (c.184C>T) in ovine CLN6 causes neuronal ceroid lipofuscinosis in Merino sheep whereas affected South Hampshire sheep have reduced levels of CLN6 mRNA. BBA-Mol. Basis. Dis. 1762, 898–905. https://doi.org/10.1016/j.bbadis.2006.09.004.

Uhlén, M., Fagerberg, L., Hallström, B.M., Lindskog, C., Oksvold, P., Mardinoglu, A., Sivertsson, Å., Kampf, C., Sjöstedt, E., Asplund, A., Olsson, I., Edlund, K., Lundberg, E., Navani, S., Szigyarto, C.A.-K., Odeberg, J., Djureinovic, D., Takanen, J. O., Hober, S., Alm, T., Edqvist, P.-H., Berling, H., Tegel, H., Mulder, J., Rockberg, J., Nilsson, P., Schwenk, J.M., Hamsten, M., von Feilitzen, K., Forsberg, M., Persson, L., Johansson, F., Zwahlen, M., von Heijne, G., Nielsen, J., Pontén, F., 2015. Proteomics. Tissue-based map of the human proteome. Science 347, 1260419. https://doi.org/10.1126/science.1260419.

Uhlen, M., Oksvold, P., Fagerberg, L., Lundberg, E., Jonasson, K., Forsberg, M., Zwahlen, M., Kampf, C., Wester, K., Hober, S., Wernerus, H., Björling, L., Ponten, F., 2010. Towards a knowledge-based human protein atlas. Nat. Biotechnol. 28, 1248–1250. https://doi.org/10.1038/nbt1210-1248.

Weleber, R.G., 1998. The dystrophic retina in multisystem disorders: the electroretinogram in neuronal ceroid lipofuscinoses. Eye 12, 580–590. https://doi.org/10.1038/eye.1998.148.

Weleber, R.G., Gupta, N., Trzupek, K.M., Wepner, M.S., Kurz, D.E., Milam, A.H., 2004. Electroretinographic and clinicopathologic correlations of retinal dysfunction in infantile neuronal ceroid lipofuscinosis (infantile Batten disease). Mol. Genet. Metabol. 83, 128–137. https://doi.org/10.1016/j.ymgme.2004.06.019.

Whiting, R.E.H., Jensen, C.A., Pearce, J.W., Gillespie, L.E., Bristow, D.E., Katz, M.L., 2016. Intracerebroventricular gene therapy that delays neurological disease progression is associated with selective preservation of retinal ganglion cells in a canine model of CLN2 disease. Exp. Eye Res. 146, 276–282. https://doi.org/10.1016/j.exer.2016.03.023.

Willett, K., Bennett, J., 2013. Immunology of AAV-mediated gene transfer in the eye. Front. Immunol. 4 https://doi.org/10.3389/fimmu.2013.00261.

Williams, R.E., Adams, H.R., Blohm, M., Cohen-Pfeffer, J.L., de Los Reyes, E., Denecke, J., Drago, K., Fairhurst, C., Frazier, M., Guelbert, N., Kiss, S., Kofler, A., Lawson, J.A., Lehwald, L., Leung, M.-A., Mikhaylova, S., Mink, J.W., Nickel, M., Shediac, R., Sims, K., Specchio, N., Topcu, M., von Löbbecke, I., West, A., Zernikow, B., Schulz, A., 2017. Management strategies for CLN2 disease. Pediatr. Neurol. 69, 102–112. https://doi.org/10.1016/j.pediatrneurol.2017.01.034.

Yin, L., Greenberg, K., Hunter, J.J., Dalkara, D., Kolstad, K.D., Masella, B.D., Wolfe, R., Visel, M., Stone, D., Libby, R.T., Diloreto, D., Schaffer, D., Flannery, J., Williams, D. R., Merigan, W.H., 2011. Intravitreal injection of AAV2 transduces macaque inner retina. Invest. Ophthalmol. Vis. Sci. 52, 2775–2783. https://doi.org/10.1167/iovs.10-6250.